3-6-2019

Lattice-driven magnetic transitions in Al(Fe,T)2X2 compounds

B. T. Lejeune
Northeastern University

Brandt A. Jensen
Ames Laboratory, brandtj@ameslab.gov

R. Barua
Northeastern University

E. Stonkevitch
Northeastern University

R. W. McCallum
McCallum Consulting LLC

See next page for additional authors

Lattice-driven magnetic transitions in Al(Fe,T)2X2 compounds

Abstract
Systematic trends connect detailed composition, lattice parameters and magnetic transition temperatures in the ferromagnetic intermetallic compound AlT2X2 with the Mn2AlB2-type crystal structure, where T = Mn, Fe, Ni, Co and X = B, C. Data were derived from both literature reports and from experiments performed on synthesized samples (T = (Fe1−xNix)2, x = 0, 0.05, 0.1; X = (B0.9C0.1)2). It is observed that compositional variation alters specific bonds responsible for the magnetic phase transition response, which ranges from 200 K ≤ *Tt* ≤ 310 K. Elemental composition that provides changes in the *c*-axis length and the associated (T-T)*c*-axis interatomic distance contribute the largest bonding effects to magnetic phase transition temperature *Tt*, alterations. Overall, these results are attributed to the dependence of *Tt* on the specifics of the Fe sublattice occupancy, electronic state and T-T bonding. In contrast, *Tt* is found to be largely independent of the (*b/a*) axial ratios and the associated (T-X)*b*-axis/(T-X)(*ac*)-plane interatomic distance ratios, indicating that interatomic interactions along the *a*-axis have little effect on the *Tt*.

Keywords
Magnetic materials, Metals, Magnetocaloric, AlFe2B2, Rare-earth-free

Disciplines
Materials Science and Engineering

Authors
B. T. Lejeune, Brandt A. Jensen, R. Barua, E. Stonkevitch, R. W. McCallum, Matthew J. Kramer, and L. H. Lewis

Lattice-driven Magnetic Transitions in $Al(Fe,T)_2X_2$ Compounds

B.T. Lejeune[a,c*], B.A. Jensen[d], R. Barua[a], E. Stonkevitch[a], R. W. McCallum[e], M.J. Kramer[d], and L. H. Lewis[a,b,c]

[a] *Department of Chemical Engineering, Northeastern University, Boston, MA 02115, USA*
[b] *Department of Mechanical and Industrial Engineering, Northeastern University, Boston, MA 02115, USA*
[c] *George J. Kostas Research Institute for Homeland Security, Northeastern University, Burlington, MA 01803, USA*
[d] *Division of Materials Sciences and Engineering, U.S. Department of Energy Ames Laboratory, Ames, IA, USA*
[e] *McCallum Consulting LLC, Santa Fe, NM, USA*

*Corresponding author: lejeune.b@husky.neu.edu

Keywords: magnetic materials, metals, magnetocaloric, $AlFe_2B_2$, rare-earth-free

Systematic trends connect detailed composition, lattice parameters and magnetic transition temperatures in the ferromagnetic intermetallic compound AlT_2X_2 with the Mn_2AlB_2-type crystal structure, where T = Mn, Fe, Ni, Co and X = B, C. Data were derived from both literature reports and from experiments performed on synthesized samples ($T = (Fe_{1-x}Ni_x)_2$, x = 0, 0.05, 0.1; $X = (B_{0.9}C_{0.1})_2$). It is observed that compositional variation alters specific bonds responsible for the magnetic phase transition response, which ranges from 200 K ≤ T_t ≤ 310 K. Elemental composition that provides changes in the *c*-axis length and the associated $(T\text{-}T)_{c\text{-axis}}$ interatomic distance contribute the largest bonding effects to magnetic phase transition temperature T_t, alterations. Overall, these results are attributed to the dependence of T_t on the specifics of the Fe sublattice occupancy, electronic state and T-T bonding. In contrast, T_t is found to be largely independent of the (*b/a)* axial ratios and the associated $(T\text{-}X)_{b\text{-axis}}/(T\text{-}X)_{(ac)\text{ -plane}}$ interatomic distance ratios, indicating that interatomic interactions along the *a*-axis have little effect on the T_t.

1. Introduction

Materials systems with strongly coupled structural and magnetic responses, sometime referred to as magnetostructural materials, allow the magnetic behavior to be tuned by structural modifications, expanding the responsiveness of their functional properties. Examples of such materials are the metamagnetic B2-type FeRh compound with a magnetic transition that is sensitive to applied pressure and elemental substitution, allowing the transition temperature to be altered from 140 K to 585 K [1–3]. Another example is the iron-arsenide superconductor $CaFe_2As_2$, which undergoes a tetragonal-to-orthorhombic phase transformation with a character that depends on the specific elemental substitution and on applied pressure to modify interatomic distances [4,5].

In this vein, intermetallic ferromagnetic compounds based on the prototypical orthorhombic Mn_2AlB_2-type structure (identified as 1-2-2 materials in this work) have received attention as a viable magnetocaloric working material by virtue of its near-room-temperature magnetostructural phase transition (T_c ~ 290 K), inexpensive chemical constituents and good magnetic cooling potential (ΔS ~ 4.4 J kg^{-1} K^{-1} @ $\mu_0 H_{app}$ = 2 T) [6–8]. While to date the estimated magnetic cooling potential of $AlFe_2B_2$ is lower than those of other contemplated magnetocaloric compounds such as $La(Fe,Mn,Si)_{13}$ (ΔS ~ 8-24 J kg^{-1} K^{-1} @ $\mu_0 H_{app}$ = 2 T), $Gd_5Ge_2Si_2$ (ΔS ~ 14 J kg^{-1} K^{-1}@ $\mu_0 H_{app}$ = 2 T), and MnFePSi (ΔS ~ 11-31 J kg^{-1} K^{-1}@ $\mu_0 H_{app}$ = 2 T), the mechanical stability, ease of production, and positive heat transfer characteristics donate continued interest in $AlFe_2B_2$-based compounds [9]. In this present study, we report new data and advance understanding to connect magnetism, bonding and composition in the AlT_2X_2 (T = Mn, Fe, Co, Ni; X = B, C) system. This work builds on earlier results that demonstrate a small but definite simultaneous change in the lattice and magnetic response of the $AlFe_2B_2$ system [8]. This knowledge allows prediction of structural and chemical conditions to trigger its inherent magnetostructural phase transition. This confirmed interplay between structure and response provides

flexibility to tailor the magnetic phase transition temperature of this system for potential application to a variety of magnetic cooling technologies [9,10].

A framework for correlating structural and magnetic properties of the AlT_2X_2 compound is constructed by examination of the bonding within the prototypical Mn_2AlB_2-type crystal structure, displayed in **Figure 1** and described below.

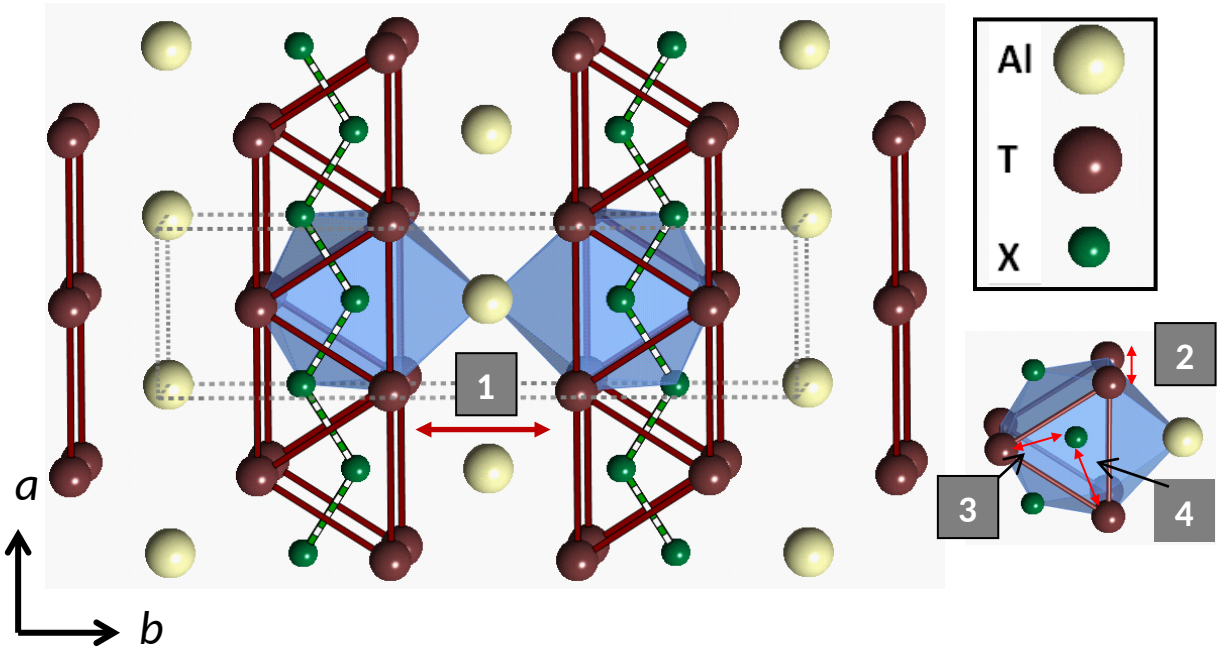

Figure 1. The orthorhombic *Cmmm*-type crystal structure of Mn_2AlB_2 consists of layers of transition-metal (T) trigonal prisms each containing a central X atom. T-X polyhedra are arranged in the (*ac*) plane and separated by an interface of Al atoms along the *b*-axis. Four key bonds labeled as 1 – 4 denote the $(T\text{-}T)_{b\text{-}axis}$, $(T\text{-}T)_{c\text{-}axis}$, $(T\text{-}X)_{b\text{-}axis}$, and $(T\text{-}X)_{(ac)\ plane}$ interatomic distances respectively and are further described in the text.

The orthorhombic Mn_2AlB_2-type crystal structure (space group *Cmmm*) consists of T_2X_2 layers within the (*ac*) plane interspersed with planes of Al atoms arranged along the uniaxial *b*-axis [11,12]. The T_2X_2 layer may be visualized as consisting of face-shared transition metal (T) trigonal prisms that surround central X atoms lying within the (*ac*) plane. The X atoms themselves form zig-zag chains within the (*ac*) plane, running through the center of the T trigonal prisms along the *a* direction [13–16]. It is asserted that the short lengths (~1.74 Å) of the X-X interatomic chains in $AlFe_2B_2$ are associated

with strongly covalent interactions [11–15]. The T_2X_2 layer and its interactions with the Al planes of atoms can be understood more completely by examining the X coordination polyhedra, shown in blue in Figure 1. These larger polyhedra are comprised of the smaller trigonal transition metal (T) prisms described earlier and include two X atoms from the adjacent face-shared trigonal prisms and the central apical Al atom of the unit cell. As introduced by Daams *et al.* and adopted by Gulay *et al*. to describe bonding within the isostructural R_2Ni_2Pb compound, the coordination number (CN) of X is 9 [17,18]. While the X coordination polyhedra contain fewer atoms than do the Al (CN = 14) and T (CN = 17) coordination polyhedra, it displays the smallest interatomic distances, ranging from 1.74-2.29 Å, and hence possesses the largest degree of near-neighbor orbital overlap, consistent with strong interatomic interactions [15,17].

Four key (T-T) and (T-X) interatomic distances, denoted Bonds 1 – 4, are identified in Figure 1 and are illustrated by double-ended arrows. Bond 1, also described as $(T\text{-}T)_{b\text{-axis}}$, is the length between the T atoms belonging to adjacent trigonal prisms that are oriented along the *b*-axis (across the Al atomic layer). Bond 2 ($(T\text{-}T)_{c\text{-axis}}$) is identified with height of the trigonal prism along the *c*-axis, enclosing the X-X chains. Bond 3 ($(T\text{-}X)_{b\text{-axis}}$) specifies the T-X interatomic distances within the X coordination polyhedra, linking the central X atom with the adjacent T atom along the *b*-axis direction. Finally, Bond 4 ($(T\text{-}X)_{(ac)\text{ plane}}$) specifies the distance from one of the T atoms lying on the edges of the 1-2-2 unit cell to the central X atom within the same X coordination polyhedra.

The layered 1-2-2 crystal structure gives rise to anisotropic magnetostructural properties within the AlT_2X_2 system [8,19]. As reported previously by ElMassalami *et al.* and Ke *et al*., the T atoms predominately influence the magnetic properties of the 1-2-2 structure [6,20]. Previous work by the current authors reported that the $AlFe_2B_2$ parent compound undergoes an anisotropic, coupled structural and magnetic (magnetostructural) phase transition near the ferromagnetic-to-paramagnetic transition temperature ($T_t \sim 290$ K) [6,8]. This transition features non-uniform changes in the *a*-, *b*-,

and *c*-parameters that deliver a conserved unit cell volume [8]. A moderate magnetocrystalline anisotropy (K ~ 1 MJ m^{-3}) is observed along the hard *c*-axis relative to that within the easy (*ab*)-plane [19,20].

The role of specific 3*d* transition-metal substitution for Fe on the crystal structure and magnetic phase transition of $AlFe_2B_2$ has been previously investigated [20–24]. Substitutions of Co and Mn are reported to lead to contraction and expansion along the *c*-axis, respectively, relative to the unmodified composition $AlFe_2B_2$; both elemental additions were found to destabilize the compounds' ferromagnetism. It is reported that the saturation magnetization and the magnetic transition temperature T_t both decrease from ~290 K to 205 K with the addition of 30 at% Co; fully suppressed ferromagnetism is noted upon incorporation of 80 at% Mn [21,22]. The results of computational studies conducted by Ke *et al.* on the $AlFe_2B_2$ compound are consistent with these experimental T_t trends and predict that the nature of the bonding along the *c*-axis plays a critical role in the ferromagnetic stability within this system. Ke *et al.'s* results further suggest that chemical modification which impacts the interatomic distances along the *c*-axis will also modify the magnetic properties of this system [20].

In this current work, the influence of transition metal (Mn, Co, Ni) substitution for Fe and of C for B on the interatomic distances and magnetic phase transition temperature (T_t) within the $AlFe_2B_2$ system is studied. It is determined that these chemical alterations do indeed exert significant influence on in-plane and out-of-plane bonding, affecting the magnetic phase transition temperature. In addition to assessment of literature data, samples of $Al_{1.2}(Fe_{1-x}Ni_x)_2B_2$ (x = 0.05, 0.10) and $Al_{1.2}Fe_2(B_{1-y}C_y)_2$ (y = 0.1) were synthesized and characterized. Analyses of both experimental and literature lattice parameter data allow identification of a systematic trend in the 1-2-2 magnetic transition temperature. These data provide quantitative assessment of the interactions between type of substituent, lattice distortion and the magnetic phase transition temperature of the AlT_2X_2 system. Understanding these effects will

facilitate tailoring the magnetic response of AlT_2X_2-type materials for prospective applications such as near-room-temperature magnetocaloric cooling [7].

2. Materials and Methods

Compositionally modified samples based on the $Al_{1.2}Fe_2B_2$ composition were made by solidification from the melt, followed by thermal treatment based on the procedure of Levin *et al.* [25]. As the $AlFe_2B_2$ compound forms via a peritectic reaction from the melt, it is necessary to add Al in excess of the stoichiometric amount to optimize the 1-2-2 phase fraction. The excess Al contributes to the formation of minority $Al_{13}Fe_4$ and FeB phases [25]. Nickel-substituted samples were produced by arc-melting together Al, $(Fe_{1-x}Ni_x)$, and B (purities > 99.9%) in a 1.2:2:2 stoichiometric ratio, with $x = 0.05$ and 0.10. These samples were homogenized by re-melting two times. Samples of composition $Al_{1.2}Fe_2B_2$ and $Al_{1.2}Fe_2(B_{0.9}C_{0.1})_2$ were synthesized via suction casting to produce rods of approximately 5 mm diameter by 4 cm length. Slabs (1 mm thickness x 3 mm width x 5 mm length) were sliced from all as-cast ingots using a low-speed diamond saw and were metallographically polished to a mirror finish in water. All slices were wrapped with tantalum foil and sealed in evacuated quartz ampoules backfilled with a partial pressure of ultra-high purity Ar for annealing at 1040 °C for 72 hours, using a heating rate of 10 °C per minute followed by furnace cooling.

The microstructure and composition of the phases present in polished samples was investigated using scanning electron microscopy and energy dispersive spectroscopy (SEM-EDS, Hitachi S4800). The Al, Fe, and Ni atomic percentages were compared for phase identification since B is not detectable through EDS. Energy-dispersive spectroscopy confirmed the nominal sample compositions.

The crystal structure and phase constitution of samples were examined with Cu-K_α X-ray diffraction (XRD, PANalytical X'Pert PRO) at room temperature in the range $10° \leq 2\theta \leq 80°$. Bragg reflections obtained from the XRD patterns were fit with a pseudo-Voight function and indexed. The lattice parameters were calculated using a least-squares cell-parameter refinement method [26]. The

interatomic distances for all AlT_2X_2 compounds studied were determined using the measured or calculated lattice parameters and the atomic positions of the parent phase where the Al sits at (0,0,0), T at (0,y_1,1/2) and X at (0,y_2,0) determined using the structure type (*Cmmm*), and have been illustrated using crystal maker (Figure 1) [11,27]. Reported variations in the atomic positions for T ($y_1 \sim 0.354$) and X ($y_2 \sim 0.207$) vary no more than ~0.1 % for T and ~0.2 % for X [11,28]. Thus the changes in the key interatomic distances (identified in the introduction) should track generally with the changes in the lattice parameters.

The ratios of selected interatomic bond distances within the structure were calculated to better understand the evolution of the crystal structure with composition. In specific, $(T\text{-}T)_{b\text{-axis}}/(T\text{-}T)_{c\text{-axis}}$ (Bond 2:Bond 1) ratios and $(T\text{-}X)_{b\text{-axis}}/(T\text{-}X)_{(ac)\text{-plane}}$ (Bond 3:Bond 4) ratios were evaluated for the samples. The latter ratio provides insight into lattice distortions associated with the (*b/a*) axial ratio. Errors in the lattice parameters and in the atomic bond length ratios are smaller than the size of the graph data markers.

Magnetic data were collected using vibrating sample magnetometry (VSM, Quantum Design model VersaLab) as a function of applied field (-3 T < $\mu_0 H_{app}$ < 3 T at T = 50 K and at 350 K) and as a function of temperature (50 K < T < 400 K at $\mu_0 H_{app}$ = 2 T). The magnetic field was applied parallel to the length of the thin sample slices and no demagnetization corrections were applied. The temperature sweep-rate for all temperature-dependent magnetic measurements was set at 2 K min^{-1}. The magnetic phase transition temperatures T_t were determined as the inflection point of the derivative of the $M(T)$ curves measured upon heating in the temperature range 50 K to 400 K at $\mu_0 H_{app}$ = 2 T. The estimated error of T_t is ±2 K. All graphs were generated using Origin Lab 8.1.

3. Results

Results regarding the structural and magnetic properties of the $Al_{1.2}(Fe_{1-x}Ni_x)_2B_2$ (x = 0, 0.05, 0.1; designated as Ni0, Ni5, Ni10 respectively) and $Al_{1.2}Fe_2(B_{0.9}C_{0.1})_2$ (designated as C10) samples

synthesized in this study are combined with analogous data derived from literature reports. This information allows deduction and validation of trends that correlate specific lattice parameter distortions with magnetic transition temperatures, facilitating prediction of transition temperatures in the AlT_2X_2 system.

3.1 Structural & magnetic character of the $Al_{1.2}(Fe_{1-x}Ni_x)_2B_2$ (x = 0.05, 0.1) and $Al_{1.2}Fe_2(B_{0.9}C_{0.1})_2$ samples synthesized in this study

In their as-solidified state, all samples are found to be multiphase in character, with a majority AlT_2X_2 phase and $Al_{13}Fe_4$ and FeB as minority phases; Fe_3C is also observed in the carbon-containing sample. After annealing, the intensities of the Bragg reflections corresponding to $Al_{13}Fe_4$ and FeB have either significantly decreased or vanished entirely, while those of the AlT_2X_2 phase have sharpened, consistent with formation of the 1-2-2 phase at the expense of $Al_{13}Fe_4$ and FeB. **Figure 2(a)** shows XRD patterns for selected $Al_{1.2}(Fe_{1-x}Ni_x)_2B_2$ and $Al_{1.2}Fe_2(B_{0.9}C_{0.1})_2$ samples as well as for $AlFe_2B_2$, $Al_{13}Fe_4$ (JCPDS 29-0042), and FeB (JCPDS 65-2599) [11].

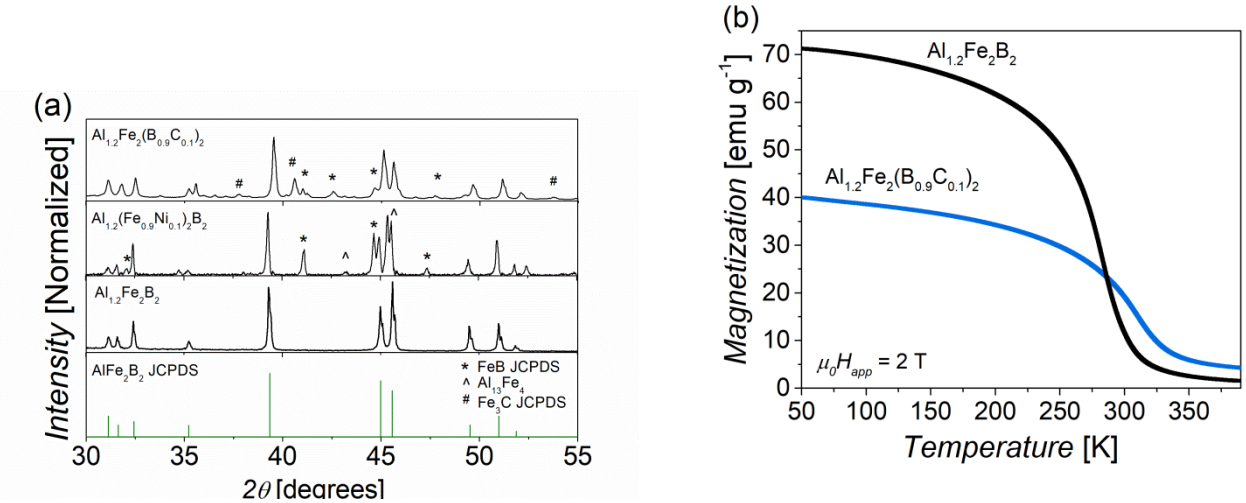

Figure 2. (a) XRD patterns for annealed $Al_{1.2}(Fe_{1-x}Ni_x)_2B_2$ (x = 0, 0.1) and $AlFe_2(B_{0.9}C_{0.1})_2$ samples with standard diffraction data included for $AlFe_2B_2$, $Al_{13}Fe_4$, FeB, and Fe_3C (b) Magnetization verses temperature curves for the Ni0 and C10 samples measured at $\mu_0 H_{app}$ = 2 T indicate an increase in the magnetic phase transition temperature from 284 K to 305 K with carbon addition.

The *a*-, *b*- and *c*-lattice constants of the 1-2-2 phase increase anisotropically (by 0.1%, 0.1% and 0.2%, respectively) with increased Ni concentration in the $Al_{1.2}(Fe_{1-x}Ni_x)_2B_2$ samples (**Table 1**), producing a

0.4% increase in the unit cell volume relative to that of the unmodified $AlFe_2B_2$ lattice. While the *c*-parameter of the 1-2-2 phase in the $Al_{1.2}Fe_2(B_{0.9}C_{0.1})_2$ sample also undergoes an expansion of 0.2%, the *a*- and *b*-parameters of the 1-2-2 phase in this sample contract (by 0.6 % and by 0.2 %, respectively) with carbon addition (Table 1) to produce a significant overall unit cell volume contraction of -0.7 %.

Table 1. Structural and magnetic data of the 1-2-2 phase present in annealed samples of compositions $Al(Fe_{1-x}Ni_x)_2B_2$ (x = 0, 0.05, 0.1) and $Al_{1.2}Fe_2(B_{0.9}C_{0.1})_2$.

Nominal composition	Sample name	T_t [K]	*a* [Å]	*b* [Å]	*c* [Å]	*V* [Å^3]
$Al_{1.2}Fe_2B_2$	Ni0	284(2)	2.924(1)	11.030(1)	2.866(1)	92.4(1)
$Al_{1.2}(Fe_{0.95}Ni_{0.05})_2B_2$	Ni5	288(2)	2.927(1)	11.041(3)	2.869(1)	92.7(1)
$Al_{1.2}(Fe_{0.9}Ni_{0.1})_2B_2$	Ni10	291(2)	2.928(1)	11.043(6)	2.871(1)	92.8(1)
$Al_{1.2}Fe_2(B_{0.9}C_{0.1})_2$	C10	305(2)	2.906(1)	11.008(1)	2.870(1)	91.8(1)

The thermomagnetic data of all annealed samples confirm a ferromagnetic-to-paramagnetic phase transition with increasing temperature; a representative plot is shown in **Figure 2(b)**. The addition of Ni to the 1-2-2 lattice produces a 60% reduction in the saturation magnetization at T = 50 K but donates an increased magnetic transition temperature from T_t = 284 K (Ni0) to T_t = 291 K (Ni10). The addition of carbon to the 1-2-2 lattice produces a similar saturation magnetization reduction (54%) at T = 50 K while also strongly enhancing the magnetic transition temperature from T_t = 284 K (Ni0) to T_t = 305 K (C10), (Figure 2(b)). These data are listed in Table 1.

3.2 Lattice and Magnetic Transition Temperature Trends in the 1-2-2 System

Data illustrating relationships between lattice distortions and magnetic transition temperatures of the AlT_2X_2 compounds, both synthesized in this work and as reported in the literature, are presented in **Figure 3** [7,21–23]. Details regarding bond length determinations and variations in the special atomic positons of the T and X atoms are described in the experimental section. A maxima in T_t is observed with respect to changes in the lattice parameters for the unmodified $AlFe_2B_2$ composition, with the largest effect observed between the *c*-parameter and T_t. To facilitate understanding of the electronic

and magnetic drivers underlying these noted lattice distortions, the magnetic transition temperature is also shown in **Figure 4** as a function of specific lattice parameter ratios and associated interatomic distance ratios.

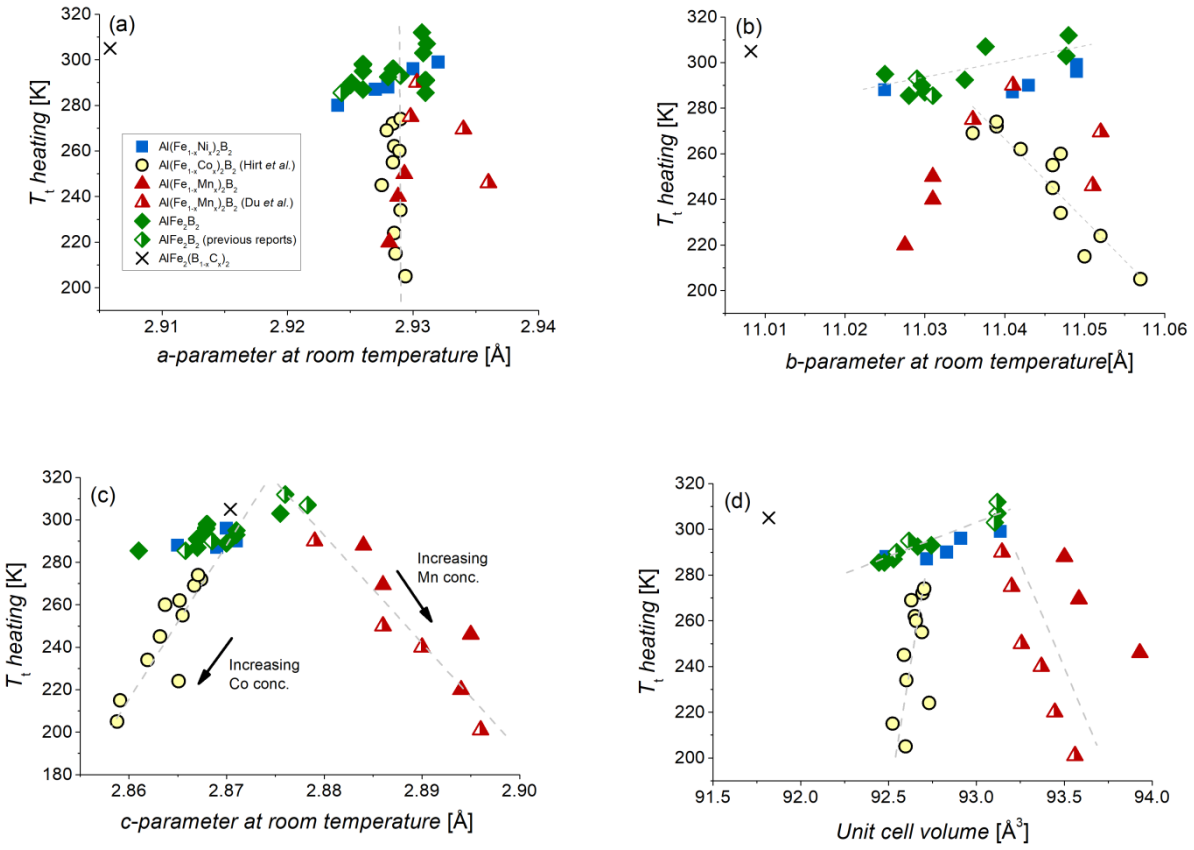

Figure 3. Magnetic transition temperature verses (a) *a*-parameter (b) *b*-parameter (c) *c*-parameter and (d) unit cell volume for ▲ $Al(Fe_{1-x}Mn_x)_2B_2$ ■ $Al(Fe_{1-x}Ni_x)_2B_2$ **X** $AlFe_2(B_{0.9}C_{0.1})_2$ ○ $Al(Fe_{1-x}Co_x)_2B_2$ ♦ $AlFe_2B_2$ compounds. Errors bars are smaller than data point markers.

As noted in Figure 3(a), the AlT_2X_2 *a*-parameters range from 2.924(2) Å – 2.936(2) Å and show little correlation with T_t (Δa_{max} = 0.4%). The carbon-substituted sample is an exception to this observed trend; it has a much smaller *a*-parameter (2.906(2) Å) and a significantly larger T_t (305 K) than those exhibited by the unmodified composition (Figure 3(a), black X symbol). Figure 3(b) displays *b*-parameters that range from 11.025(2) Å – 11.057(2) Å (Δb_{max} = 0.3%). As before, the carbon-

substituted sample possesses a significantly smaller *b*-parameter (*b* = 11.008(2) Å) combined with an enhanced T_t. The Co-containing samples show a strong decrease in T_t with increased *b*-parameter while all other AlT_2X_2 samples exhibit a minor dependence of T_t on the *b*-parameter magnitude. The *c*-parameter values shown in Figure 3(c) range from 2.859(2) Å – 2.896(2) Å (Δc_{max} = 1.3%), and exhibit the strongest effect on T_t among the three 1-2-2 orthorhombic lattice parameters. This trend is strongly dependent on the identity of the specific substitutional element: cobalt incorporation reduces the *c*-parameter while manganese additions increase it. In both circumstances the magnetic transition temperature T_t is decreased from the maximum values characterizing the parent $AlFe_2B_2$ phase. Figure 3(d) presents the AlT_2X_2 unit cell volumes which range from 92.5(1) Å^3 – 93.9(1) Å^3 (ΔV_{max}= 1.5%); again the carbon-substituted sample possesses a significantly different unit cell volume value of *V* = 91.8(1) Å^3 (Figure 3(d)). The trends of the magnetic transition temperature with unit cell volume (Figure 3(d)) closely echo those involving the *c*-parameter, Figure 3(c).

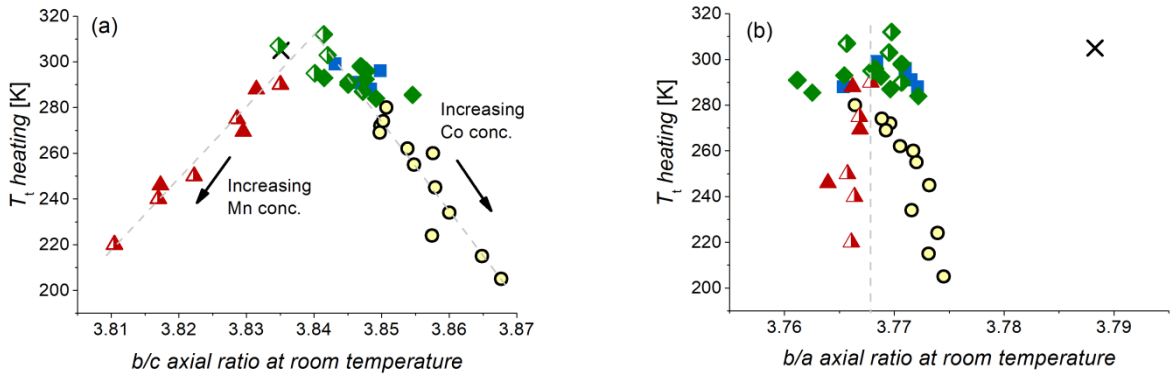

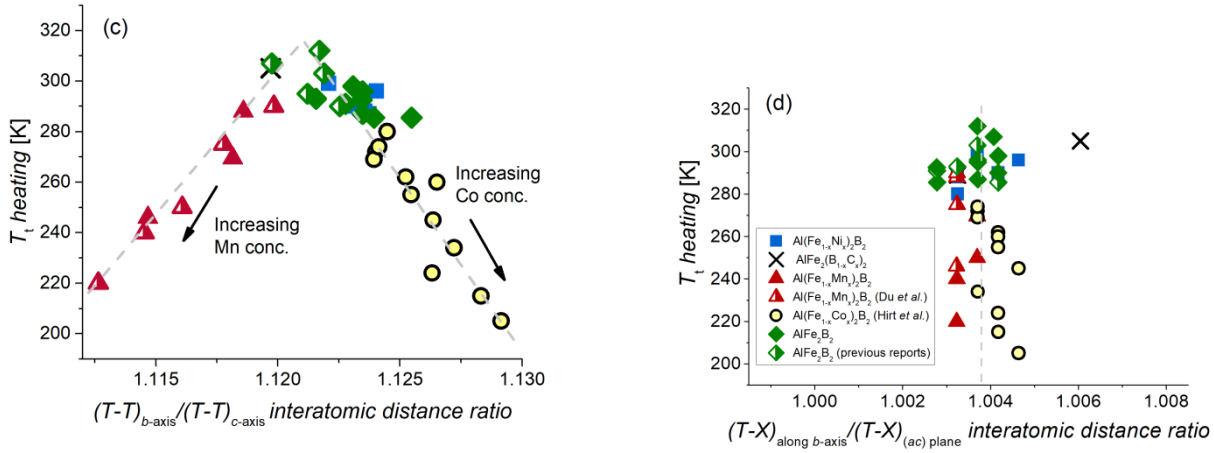

Figure 4. AlT_2X_2 magnetic transition temperature versus (a) (*b/c*) and (b) (*b/a*) axial ratios as well as the ratio of (c) $(T\text{-}T)_{b\text{-axis}}/(T\text{-}T)_{c\text{-axis}}$ and (d) $(T\text{-}X)_{\text{along } b\text{-axis}}/(T\text{-}X)_{(ac)\text{-plane}}$ interatomic distances for ▲ $Al(Fe_{1-x}Mn_x)_2B_2$ ■ $Al(Fe_{1-x}Ni_x)_2B_2$ **X** $AlFe_2(B_{0.9}C_{0.1})_2$ ○ $Al(Fe_{1-x}Co_x)_2B_2$ ♦ $AlFe_2B_2$ compounds. Errors bars are smaller than data point markers.

In addition to presenting specific lattice parameter behavior, selected axial ratios are correlated with magnetic transition temperatures T_t in Figure 4 to more strongly illustrate competitive interactions between inequivalent in-plane and out-of-plane lattice distortions. These data are derived both from experimental work presented here and from existing literature. The (*b/c*) axial ratios (Figure 4(a)) provide information concerning out-of-plane 1-2-2 lattice distortions traversing the Al layer, separating the face-shared X-atom coordination polyhedra, while the (*b/a*) axial ratios (Figure 4(b)) represent (*ac*)-plane distortions within the X-atom coordination polyhedra (see Figure 1). Figure 4(a) indicates that T_t increases quasi-linearly with increasing (*b/c*) axial ratio to reach a maximum at T_t = 312 K at a (*b/c*) ratio of 3.840(3) that characterizes the unmodified parent $AlFe_2B_2$ phase. For yet larger (*b/c*) axial ratios realized upon cobalt and nickel substitution, T_t decreases in a quasi-linear fashion to reach a minimum at T_t = 205 K at (*b/c*) ~ 3.870(3). In contrast to the strong correlation between the (*b/c*) axial ratio and T_t, the (*b/a*) axial ratios show little correlation with T_t, Figure 4(b); these ratios (with the exception of that of the C-substituted sample) fall in a narrow band of values ranging from 3.761(3) to 3.774(3) (± 0.2 % deviation from the median). The interatomic distance ratio $(T\text{-}T)_{b\text{-axis}}/(T\text{-}T)_{c\text{-axis}}$ of Figure 4(c), which depicts interatomic distances contributing to the (*b/c*) axial ratio as introduced

earlier (Bonds 1 and 2 of Figure 1), show a similar T_t dependence, with a maximum value of ~ 1.122(1) and a minimum value of ~ 1.129(1). The $(T\text{-}X)_{(b)\text{-axis}}/(T\text{-}X)_{(ac)\text{-plane}}$ interatomic distance ratio trend (Figure 4(d)), analogous to the (b/a) axial ratio trend and consisting of Bonds 3 and 4 of Figure 1, shows little correlation with T_t; rather it exhibits a tight clustering of data points ranging from ~ 1.003(1) to 1.005(1) (±0.1 % deviation from the median), with the C-containing sample lying outside of this band.

4. Analysis and Discussion

Examination of the AlT_2X_2 system data and trends previously presented allows development of an empirical trend that describes systematic interactions between the magnetic transition temperature (T_t) and for the magnetic state. The in-plane and out-of-plane interatomic distances of the $AlMn_2B_2$ crystal structure, defined in Section 2.2, may be considered as proxies for the strength of electronic interactions in this system, reflecting the origins of the coupling between structure and magnetism. Carbon substitution for boron illustrates how (X-X) and (T-X) bond alterations in the 1-2-2 system affect the *a*-parameter but not T_t which is mainly dictated by (T-T) bonding.

4.1 In-plane *vs.* out-of-plane interactions in AlT_2X_2

The data displayed in Figure 3 confirm that the AlT_2X_2 structure is extraordinarily sensitive to precise composition: incorporation of *3d* transition metals (Mn, Fe, Co, Ni) for T and C for X result in rather small alterations in the lattice parameters (< 0.037 Å) but deliver significant magnetic transition temperature (T_t) alterations, providing a very broad magnetic transition temperature range of 205 K to 312 K. Lattice expansion along the *c*-axis enhances T_t in AlT_2X_2 compositions that do not contain Mn; in fact, the *c*-parameter largely determines T_t, with the *b*-parameter relegated to a secondary role. Accordingly, T_t is largely determined by the direct $(T\text{-}T)_{c\text{-axis}}$ interatomic distances (Bond 2 in Figure 1) within the X coordination polyhedra. This conclusion is consistent with previous reports that the *c*-axis in the $AlFe_2B_2$ composition undergoes the largest change through the magnetic phase transition

[8,20]. Additionally, as Mn is substituted for Fe in the $AlFe_2B_2$ composition, both $(T\text{-}T)_{b\text{-axis}}$ and $(T\text{-}T)_{c\text{-axis}}$ interatomic distances increase but in a disparate manner, delivering an overall decrease in both the $(T\text{-}T)_{b\text{-axis}}/(T\text{-}T)_{c\text{-axis}}$ ratio (Figure 4(c)) and in the magnetic transition temperature. This result signals the development of antiferromagnetic interactions between Mn and Fe atoms, as described by Ke *et al.* and suggested by Chai *et al.* for the $AlMn_2B_2$ compound [20,22]. In contrast, incorporation of Co causes the (T-T) interatomic distances along both the *b*- and *c*-axes to decrease disproportionately, delivering an increased $(T\text{-}T)_{b\text{-axis}}/(T\text{-}T)_{c\text{-axis}}$ ratio but also reducing T_t from its maximum value [20].

In addition to bonding modification, electronic effects likely also contribute to the observed effects reported here. Insight regarding these electronic effects may be gained from the work of Ke *et al*. and Kadas *et al*. who performed computational studies relating the electronic structure and magnetic properties in compositional variants of $AlFe_2B_2$ [20,29]. Specifically, Ke *et al*. used density functional theory to study the electronic structure and intrinsic magnetic properties of the Fe_2AlB_2 compound. They found that electron doping modifies the density of states (DOS) of the minority spin channel near the Fermi level, which decreases the magnetic moment on the Fe sites. Similarly, Kadas *et al.* determined that metal-metal bond strength in AlM_2B_2 (M = Cr, Mn, Fe, Co, Ni) compounds decreased with increased electron doping, a result attributed to filling of the antibonding states as the *3d* band occupancy increases.

A rather large distribution of lattice parameters ($2.924 \leq a \leq 2.931$ Å; $11.025 \leq b \leq 11.048$ Å; $2.861 \leq c \leq 2.878$ Å) and magnetic transition temperatures ($285.5 \leq T_t \leq 312$ K) are reported in the literature for $AlFe_2B_2$. This wide variation may be attributed to the rate of solidification from the melt and to the mode(s) of subsequent processing. These procedures are contemplated to contribute to different antisite occupancies, producing variations in the 1-2-2 *b*-axis and in the associated $(T\text{-}T)_{b\text{-axis}}$ interatomic distances (Bond 1 in Figure 1).The $(T\text{-}T)_{b\text{-axis}}$ interatomic distance traverses the Al atom

layer within the (*ac*)-plane, suggesting that Al and T atom antisite occupancy or Al-site vacancies could alter the Al layer spacing resulting in the distribution of the structural and magnetic properties observed for $AlFe_2B_2$. This conclusion is supported by, for example, the noted differences in T_t reported for arc-melted (T_t ~ 290 K) and melt-spun (T_t = 312 K) samples of $Al_{1.2}Fe_2B_2$ nominal composition [24,25].

4.2 Effect of carbon substitution on the AlT_2X_2 lattice and (X-X) bonding

Carbon additions to the 1-2-2 structure are especially interesting: they significantly increase the magnetostructural transition temperature (T_t) relative to that of the unmodified composition, while at the same time reduce the unit cell volume. This unit cell volume reduction results from contraction of the *a*- and *b*- parameters relative to those of the unmodified composition, irrespective of the expansion observed along the *c*-axis. The magnitude of the *a*-axis contraction in the $Al_{1.2}Fe_2(B_{0.9}C_{0.1})_2$ unit cell achieved by substitution of 10 at.% C for B is three times larger than that of the *b*-axis (0.6 % *vs*. 0.2 %, respectively). The simultaneous expansion along the *c*-axis (Δc_{max} = 0.2%) and increase in T_t of $Al_{1.2}Fe_2(B_{0.9}C_{0.1})_2$ relative to the unmodified sample is consistent with the behavior of compositionally modified $AlFe_{2-x}T_xB_2$ samples. The enhancement of T_t in the $Al_{1.2}Fe_2(B_{0.9}C_{0.1})_2$ sample irrespective of the lattice contraction along the *a*- and *b*- axes highlights that the lattice contribution to T_t is strongest along the *c*-axis of AlT_2X_2 compounds.

Examination of bonding in compounds with structures related to the 1-2-2 structure help to explain why carbon incorporation alters the AlT_2X_2 *a*-parameter but has little effect on T_t. For example, FeB and $AlFe_2B_2$ have similar structures, as both contain face-shared Fe atom trigonal prisms containing a central B atom with the B-B bonds forming zig-zag chains along the *a*-axis (structure of $AlFe_2B_2$ shown in Figure 1) [15]. Reports examining B-B and Fe-B bonding within the orthorhombic FeB crystal structure (space group *Pnma*) conclude that altering the B concentration predominately alters the strength of (B-B) bonds along the *a*-axis to modify the *a*-parameter [15,30,31]. Bonding in FeB is

stronger between like atoms ((B-B) and (Fe-Fe)) than between dissimilar atoms ((Fe-B)$_{b\text{-axis}}$ and (Fe-B)$_{(ac)\text{-plane}}$) [15,30]. Therefore as the strength of (B-B) bonds change this has a minor effect on the Fe sublattice and (Fe-Fe) bonds in iron borides [15]. Analogously, C substitution in AlT_2X_2 mainly alters (X-X) bonds causing variations in the *a*-parameter but has little effect the (T-T)$_{c\text{-axis}}$ bonding responsible for T_t variations.

5. Conclusions

Analyses of both experimental and literature lattice parameter data provide quantitative guidance for understanding the interplay between type of substituent, lattice distortions and the magnetic phase transition temperature of the AlT_2X_2 system over a broad range of T and X (T = Mn, Fe, Co, Ni; X = B, C) compositions. The AlT_2X_2 structure is extraordinarily sensitive to composition: incorporation of *3d* transition metals (Mn, Fe, Co, Ni) for T and C for X result in rather small alterations in the lattice parameters (< 1.3 %) but significant magnetic transition temperature (T_t) alterations, providing a very broad magnetic transition temperature range of 205 K to 312 K. It is found that Ni and C incorporation increase the *c*-parameter and the T_t relative to $AlFe_2B_2$. In contrast to the minor expansion in the *a*- and *b*-parameters with Ni substitution, 10 at.% C substitution for B donates a 0.6% and 0.2% decrease in the *a*- and *b*-parameters respectively. It is deduced that the (*b/c*) axial ratio and associated (T-T)$_{b\text{-axis}}$/(T-T)$_{c\text{-axis}}$ interatomic distance ratio dictate the magnetic transition temperature mainly due to the *c*-axis and underlying (T-T)$_{c\text{-axis}}$ distances. In contrast, the magnetic transition temperature is largely independent of the (*b/a)* axial ratio and the associated (T-X)$_{b\text{-axis}}$/(T-X)$_{(ac)\text{ -plane}}$ interatomic distance ratio. Overall, these results are attributed to the dependence of T_t on the specifics of the Fe sublattice occupancy, electronic state and T-T bonding.

The proposed empirical trend may hold technological relevance in designing the next generation of rare-earth-free magnetic cooling materials by providing an assessment of the interactions between the 1-2-2 lattice and magnetic transition temperatures within the AlT_2X_2 system over a large operating

temperature range spanning 200-320 K to accommodate cooling applications that employ a cascaded design of compositionally graded materials. Alternative synthesis methods involving application of a tensile force along the *c*-axis of crystallographically-oriented bulk samples or epitaxially grown thin film samples may be additional mechanisms for transition temperature modification within the $AlFe_2B_2$ system.

Acknowledgements

Funding and resources for this research was provided for by Northeastern University and the U.S Department of Energy (DOE), Advanced Research Projects Agency – Energy (DE-AR00000754).

Conflict of Interest: None

References

[1] R. Barua, F. Jiménez-Villacorta, L.H. Lewis, Towards tailoring the magnetocaloric response in FeRh-based ternary compounds, J. Appl. Phys. 115 (2014) 17A903. doi:10.1063/1.4854975.

[2] R. Barua, I. McDonald, F. Jiménez-Villacorta, D. Heiman, L.H. Lewis, Multivariable tuning of the magnetostructural response of a Ni-modified FeRh compound, J. Alloys Compd. 689 (2016) 1044–1050. doi:10.1016/j.jallcom.2016.08.004.

[3] M.G. Loving, R. Barua, C. Le Graët, C.J. Kinane, D. Heiman, S. Langridge, C.H. Marrows, L.H. Lewis, Strain-tuning of the magnetocaloric transition temperature in model FeRh films, J. Phys. D. Appl. Phys. 51 (2018). doi:10.1088/1361-6463/aa9d1f.

[4] N. Ni, S. Nandi, a. Kreyssig, a. Goldman, E. Mun, S. Bud'ko, P. Canfield, First-order structural phase transition in CaFe2As2, Phys. Rev. B. 78 (2008) 14523. doi:10.1103/PhysRevB.78.014523.

[5] T. Park, E. Park, H. Lee, T. Klimczuk, E.D. Bauer, F. Ronning, J.D. Thompson, Pressure-induced superconductivity in CaFe 2 As 2, J. Phys. Condens. Matter. 20 (2008) 322204. doi:10.1088/0953-8984/20/32/322204.

[6] M. ElMassalami, D.D.S. Oliveira, H. Takeya, On the ferromagnetism of AlFe2B2, J. Magn. Magn. Mater. 323 (2011) 2133–2136. doi:10.1016/j.jmmm.2011.03.008.

[7] X. Tan, P. Chai, C.M. Thompson, M. Shatruk, Magnetocaloric Effect in AlFe2B2: Toward Magnetic Refrigerants from Earth-Abundant Elements, J. Am. Chem. Soc. 135 (2013) 9553–9557. http://pubs.acs.org/doi/abs/10.1021/ja404107p (accessed December 1, 2014).

[8] L.H. Lewis, R. Barua, B. Lejeune, Developing magnetofunctionality: Coupled structural and magnetic phase transition in AlFe 2 B 2, J. Alloys Compd. 650 (2015) 482–488. doi:10.1016/j.jallcom.2015.07.255.

[9] V. Franco, J.S. Blázquez, B. Ingale, a. Conde, The Magnetocaloric Effect and Magnetic

Refrigeration Near Room Temperature: Materials and Models, Annu. Rev. Mater. Res. 42 (2012) 305–342. doi:10.1146/annurev-matsci-062910-100356.

[10] A. Kitanovski, J. Tušek, U. Tomc, U. Plaznik, M. Ožbolt, A. Poredoš, Magnetocaloric Materials for Freezing, Cooling, and Heat-Pump Applications, in: Magnetocaloric Energy Convers., Springer international publishing, 2015: pp. 23–38. doi:10.1007/978-3-319-08741-2.

[11] W. Jeitschko, The crystal structure of Fe2AlB2, Acta Crystallogr. B25 (1969) 163–165. doi:10.1107/S0567740869001944.

[12] R. Hoffmann, C. Zheng, Making and breaking bonds in the solid state: The ThCr2Si2 structure, J. Phys. Chem. 89 (1985) 4175–4181.

[13] P. Rogl, H. Nowotny, XII. Ternary Metal Borides, in: V.I. Matkovich (Ed.), Boron Refract. Borides, Springer-Verlag Berlin Heidelberg, New York, 1977: pp. 413–443.

[14] P. Rogl, H. Nowotny, Structural chemistry of ternary borides, J. Less-Common Met. 61 (1978) 39–45.

[15] D. Joyner, O. Johnson, D.M. Hercules, D.W. Bullett, J.H. Weaver, Study of the iron borides. IV. Relation of bonding to structure and magnetic behavior from photoemission experiments and ab initio calculations, Phys. Rev. B. 24 (1981) 3122–3137.

[16] T. Lundstrom, Structure , defects and properties of some refractory borides Fig ., Pure Appl. Chem. 57 (1985) 1383–1390.

[17] J.L.C. Daams, P. Villars, J.H.. van Vucht, Atlas of crystal structure types for intermetallic phases, ASM International, 1991.

[18] L.D. Gulay, Y.. Kalychak, M. Wolcyrz, Crystal structure of R2Ni2Pb (R = Y, Sm, Gd, Tb, Dy, Ho, Er, Tm, Lu) compounds, J. Alloys Compd. 311 (2000) 228–233.

[19] R. Barua, B.T. Lejeune, L. Ke, G. Hadjipanayis, E.M. Levin, R.W. McCallum, M.J. Kramer, L.H. Lewis, Anisotropic magnetocaloric response in AlFe2B2, J. Alloys Compd. 745 (2018) 505–512. doi:10.1016/j.jallcom.2018.02.205.

[20] L. Ke, B.N. Harmon, M.J. Kramer, Electronic structure and magnetic properties in T2AlB2 (T = Fe, Mn, Cr, Co, and Ni) and thier alloys, Phys. Rev. B. 95 (2017) 1–9.

[21] S. Hirt, F. Yuan, Y. Mozharivskyj, H. Hillebrecht, AlFe2-xCoxB2 (x=0-0.30): Tc Tuning through Co Substitution for a Promising Magntocaloric Material Realized by Spark Plasma Sintering, Inorg. Chem. 55 (2016) 9677–9684. doi:10.1021/acs.inorgchem.6b01467.

[22] P. Chai, S. a. Stoian, X. Tan, P. a. Dube, M. Shatruk, Investigation of magnetic properties and electronic structure of layered-structure borides AlT2B2 (T=Fe, Mn, Cr) and AlFe2–xMnxB2, J. Solid State Chem. 224 (2015) 52–61. doi:10.1016/j.jssc.2014.04.027.

[23] Q. Du, G. Chen, W. Yang, J. Wei, M. Hua, Magnetic frustration and magnetocaloric effect in AlFe2-xMnxB2 (x=0-0.5) ribbons, J. Phys. D. Appl. Phys. 335001 (2015) 1–6. doi:10.1088/0022-3727/48/33/335001.

[24] Q. Du, G. Chen, W. Yang, Z. Song, M. Hua, H. Du, Magnetic properties of AlFe2B2 and CeMn2Si2 synthesized by melt spinning of stoichiometric compositions, Jpn. J. Appl. Phys. 53003 (2015) 1–5.

[25] E.M. Levin, B.A. Jensen, R. Barua, B. Lejeune, A. Howard, R.W. McCallum, M.J. Kramer, L.H. Lewis, Effects of Al content and annealing on the phases formation, lattice parameters, and magnetization of AlxFe2B2 (x = 1.0, 1.1, 1.2) alloys, Phys. Rev. Mater. 2 (2018) 1–9. doi:10.1103/PhysRevMaterials.00.004400.

[26] G.A. Novak, A.A. Colville, A practical interactive least-squares cell-parameter program using an electronic spreadsheet and a personal computer, Am. Mineral. 74 (1989) 488–490.

[27] K. Momma, F. Izumi, VESTA 3 for three-dimensional visualization of crystal, volumetric and morphology data, J. Appl. Crystallogr. 44 (2011) 1272–1276.

[28] V.H.J. Becher, K. Krogmann, E. Peisker, Uber das ternare Borid Mn2AlB2, Zeitschrift Fur Anorg. Und Allg. Chemie. (1966) 140–147.

[29] K. Kadas, D. Lusan, J. Hellsvik, J. Cedervall, P. Berastegui, M. Sahlberg, U. Jansson, O. Erijsson, AlM2B2 (M = Cr , Mn , Fe , Co , Ni): a group of nanolaminated materials, J. Phys. Condens. Matter. 29 (2017) 1–11.

[30] R.S. Perkins, P.J. Brown, Charge and spin density in the iron borides, J. Phys.F Met. Phys. 4 (1974) 906–920.

[31] O. Johnson, D. Joyner, D.M. Hercules, A Study of the Iron Borides 2. Electronic Structure, J. Phys. Chem. 84 (1980) 542–547. doi:10.1021/j100442a020.

Figure 1. The orthorhombic Cmmm-type crystal structure of Mn2AlB2 consists of layers of transition-metal (T) trigonal prisms each containing a central X atom. T-X polyhedra are arranged in the (ac) plane and separated by an interface of Al atoms along the b-axis. Four key bonds labeled as 1 – 4 denote the (T-T)b-axis, (T-T)c-axis, (T-X) b-axis, and (T-X)(ac) plane interatomic distances respectively and are further described in the text.

Figure 2. (a) XRD patterns for annealed $Al_{1.2}(Fe_{1-x}Ni_x)_2B_2$ (x = 0, 0.1) and $AlFe_2(B_{0.9}C_{0.1})_2$ samples with standard diffraction data included for $AlFe_2B_2$, $Al_{13}Fe_4$, FeB, and Fe_3C (b) Magnetization verses temperature curves for the Ni0 and C10 samples measured at $\mu_0 H_{app}$ = 2 T indicate an increase in the magnetic phase transition temperature from 284 K to 305 K with carbon addition.

Figure 3. Magnetic transition temperature verses (a) *a*-parameter (b) *b*-parameter (c) *c*-parameter and (d) unit cell volume for ▲ $Al(Fe_{1-x}Mn_x)_2B_2$ ■ $Al(Fe_{1-x}Ni_x)_2B_2$ **X** $AlFe_2(B_{0.9}C_{0.1})_2$ ○ $Al(Fe_{1-x}Co_x)_2B_2$ ♦ $AlFe_2B_2$ compounds. Errors bars are smaller than data point markers.

Figure 4. AlT_2X_2 magnetic transition temperature versus (a) (*b/c*) and (b) (*b/a*) axial ratios as well as the ratio of (c) $(T\text{-}T)_{b\text{-axis}}/(T\text{-}T)_{c\text{-axis}}$ and (d) $(T\text{-}X)_{\text{along } b\text{-axis}}/(T\text{-}X)_{(ac)\text{-plane}}$ interatomic distances for ▲ $Al(Fe_{1-x}Mn_x)_2B_2$ ■ $Al(Fe_{1-x}Ni_x)_2B_2$ **X** $AlFe_2(B_{0.9}C_{0.1})_2$ ○ $Al(Fe_{1-x}Co_x)_2B_2$ ♦ $AlFe_2B_2$ compounds. Errors bars are smaller than data point markers.